CHALLENGES IN EUROPEAN AEROSPACE
5TH CEAS AIR & SPACE CONFERENCE

CEAS

DAMAGE IDENTIFICATION IN COMPOSITE PANELS USING GUIDED WAVES

R. Loendersloot
University of Twente - Faculty of Engineering Technology, chair of Dynamics Based Maintenance
Assistant Professor
P.O. Box 217, 7500AE, Enschede, The Netherlands
r.loendersloot@utwente.nl
M. Moix-Bonet
German Aerospace Center - Institute of Composite Structures and Adaptive Systems
Research Assistant
Lilienthalplatz 7, 38108, Braunschweig, Germany
maria.moix-bonet@dlr.de

ABSTRACT

A methodology for the identification of barely visible impact damage using guided waves on a typical aircraft composite structure is implemented. Delaminations and debondings have been introduced in two stiffened panels by means of impact loads. Various different impact locations were selected to assess the performance of the identification methods for different conditions. The two structures were interrogated beforehand and afterwards with an integrated piezo-electric wave active sensor network. On top of that, preliminary results from a door-surrounding structure, manufactured by the project-partners, are analysed. A graphical user interface is developed to visualise the potentially damaged area(s). The interface allows, on top of detection, an assessment of the location and severity of the damage, without requiring in-depth knowledge of wave propagation theory. Hence, a fast, on-site assessment can be performed. The software also allows for a more detailed offline analysis. A series of damage indicator algorithms is implemented to assess the performance of these for various cases, revealing the most suitable parameters for the given structure and damage types. The visualisation software allows to focus on specific areas, enhancing the analysis of multiple damages in a structure. The results of the damage identification, in terms of size and location of the damage, are compared to the size and location as retrieved from C-scan images. The damage identification software tool is shown to be a powerful instrument in both the quick, on-site damage assessment and the understanding of the effects of various damage scenarios on the time response data. The output is a valuable input for (model assisted) probability of detection methods.

1 INTRODUCTION

Operational cost in aviation is an important factor of the total cost of an aircraft. These cost can be divided in direct maintenance cost and indirect costs due to unscheduled maintenance time. Uncertainties regarding the behaviour and current state of components negatively influence these costs, necessary to guarantee safe operation of the aircraft. The introduction of composite materials, justified by their high specific stiffness and good fatigue and corrosion resistance, also introduced more uncertainties: composite laminates are prone to suffer from delaminations as well ass barely visible impact damages (BVID). The impact damage proneness is currently addressed with a damage tolerant design and an increase of Non-Destructive Inspections (NDI). Structural Health Monitoring (SHM) is envisioned to complement NDIs, resulting in a decrease of the maintenance cost, while guaranteeing the aircrafts safety. The objective of Application Scenario 6 of the EU FP7 project "Smart Intelligent Aircraft Structures" (SARISTU) is to develop a tool to assess an impact damage in a composite structure. The assessment relies on the use of a network integrated ultrasonic transducers and the composites structures under investigation are representative for a door-surrounding structure. Acousto-ultrasonic guided waves are actuated and received by this network, providing information on the structural integrity of the component. A reliable damage identification procedure is currently under development such that acousto-ultrasonics become a feasible alternative for NDI in aircraft structures.
A graphical tool is considered to be of significant importance for the development of an SHM-tool:

the tool has to have the functionality to support the inspection process and decision making process regarding maintenance and repair of structures. The graphical user interface (GUI) should allow the user to analyse data, choosing various options related to the type of analysis, region of interest, while not requesting in-depth knowledge on the algorithms implemented. It should also provide a clear output to be used in for example (Model Assisted) Probability of Detection - (MA)PoD - analysis [1]. Visualisation of the data and the potentially damaged area is an important element in the user interface.
The main principle of the damage assessment is that an ultrasonic guided wave signal is used to interrogate the structure. Here, this implies a windowed wave packet containing a limited number ($\sim$3-10) of sine waves with a frequency in the order of 50-500 kHz. The signal is subsequently registered by a sensor positioned at some distance from the actuator. The way the signal is altered while travelling through the material forms the base of the damage assessment. A network of Piezoelectric Wafer Active Sensors (PWAS) is employed, where the transducers sequentially act as actuator, while all others act as sensors. The term *workspace* is used here to refer for this set of transducers. Each straight line between two transducers is referred to as a *path*. A full coverage of paths for the area enclosed by the transducers is obtained by alternating the actuator, a method know as "Reconstruction Algorithm for Probabilistic Inspection of Defects" (RAPID) [2]. Note that each path provides information on the possible presence of damage close to the path, but only the combination of paths provides sufficient information to localise potentially damaged spots. This is partly caused by the reversibility assumption: it is assumed that switching the actuator and sensor for a path does not affect the resulting signal. Strictly taken, this assumption only holds for the pristine situation, since a damage will introduce non-linearities [3]. The assumption implies that the signal does not hold any information on the location of the possible damage on the path; each path is only measured once at actuation frequency.
This type of damage identification in aircraft structures has been extensively reported in the literature over the past decade. Matt et al. [4] monitored the bonded joint of a wing-to-spar with ultrasonic guided waves. Their work comprises numerical and experimental work, but is confined to bond defects. Zhao et al. [5] detected and localised rivet cracks and corrosion on an aircraft aluminium wing. They used a network of transducers and the RAPID algorithm to localise the damage and concluded the algorithm works effectively for the relatively small and low complexity structure they investigated. Wu [6] investigated a number of damage diagnostic imaging algorithms, based on measurements with the SMARTLayer® system integrated in flat composite plates with and without T-stringers. Their work discusses a large amount of experimental data. Their main result is the observation that the use of multiple frequencies (all S_0-mode) enhances the localisation of the damage.
These references are representative for the current state of art: despite the numerous studies, a method that achieves a reliable damage assessment on large composite structures with complex geometries has yet to be developed. The challenges are on the one hand the multiple wave modes in the material, wave reflection, wave conversions and non-isotropic behaviour or high wave attenuation and on the other hand the best ways to capture all this in an easy to use software. This research is therefore directed to the development of a damage identification methodology, including a graphical representation, of large, complex, composite structures. Small scale panels and a full scale door-surrounding structure, to which realistic BVIDs are applied, are used in this project. A probability-based diagnostic imaging methodology based on several damage indices and actuation frequencies is implemented in a software with a graphical user interface, providing the possibility for a fast analysis, combined with the possibility to assess the results in more detail. Finally, it should be possible to identify BVIDs, effectively translated to delaminations, with a minimum radius 20$\pm$5 mm: all smaller delaminations are in principle considered to be too small to be detected reliably, but all larger delaminations are expected to be found as they pose a safety risk for the component. The accuracy in location is specified to be $\pm$10 mm.

2 TEST PANELS

Two identical composite structures, each with three co-bonded Ω-stringer and 40 co-bonded piezo-electric transducers were manufactured. The skin (1500$\times$750 mm^2), with a thickness of 2 mm, has a quasi-isotropic layup and is slightly curved (R_{outer} =2075 mm). The stringers have a constant Ω-shaped cross-section (2 mm thickness, quasi-isotropic layup). A schematic of the panel design with a detail of

the stringer is shown in fig. 1.

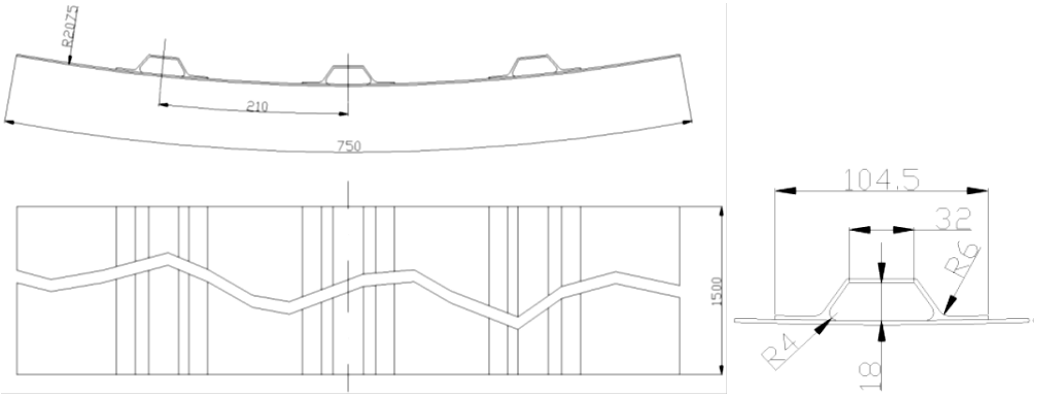

Figure 1: *Design of the carbon fibre reinforced panel [7].*

One panel is equipped with SMARTLayer® transducers, whereas the other is equipped with DuraAct™ transducers. The co-bonding process, as well as the durability of both transducer types have been studied by Moix-Bonet et al. [8]. The network is arranged in a total of 8 arrays containing 5 transducers each. The arrays are positioned parallel to the stringers, while the distance between two transducers equals 120 mm in the direction parallel to the stringers and 200 mm in perpendicular direction. The structure with the co-bonded SMARTLayer® piezoelectric transducers is depicted in fig. 2.

Figure 2: *Stiffened composite structure with 40 co-bonded SMARTLayer® transducers [9].*

Next to these test panels, a full scale door surrounding structure (see fig. 3) is manufactured by the SARISTU partners [10]. The structure is equipped with over 500 transducers (mostly sensor based on DuraAct™ technology, but further developed by the SARISTU partners mentioned). The panel measures 3.5 meters in height and 5.5 meters in width, a series of Ω-stringers are co-bonded, spaced similarly as the test panels. The distance between the transducers is therefore also similar.
The impact campaign for the curved panels consisted of several impacts introduced from the outer skin in each test panel with energies in the range of 20-34 Joules using a hemispherical projectile with a diameter of 25 mm is. The impact energies target BVIDs and de-bondings with an area between 518 mm^2 and 690 mm^2. The diameter of a round damage with this area measures 27.6±2 mm. The defects introduced were measured with traditional NDI methods, which serve as a reference to determine the performance of the damage identification algorithms. The geometry (top view), transducer network and impact positions in one of the test pieces, as well as two representative NDI images of defects are shown in fig. 4.

Figure 3: *Door surrounding structure equipped with over 500 transducers [10].*

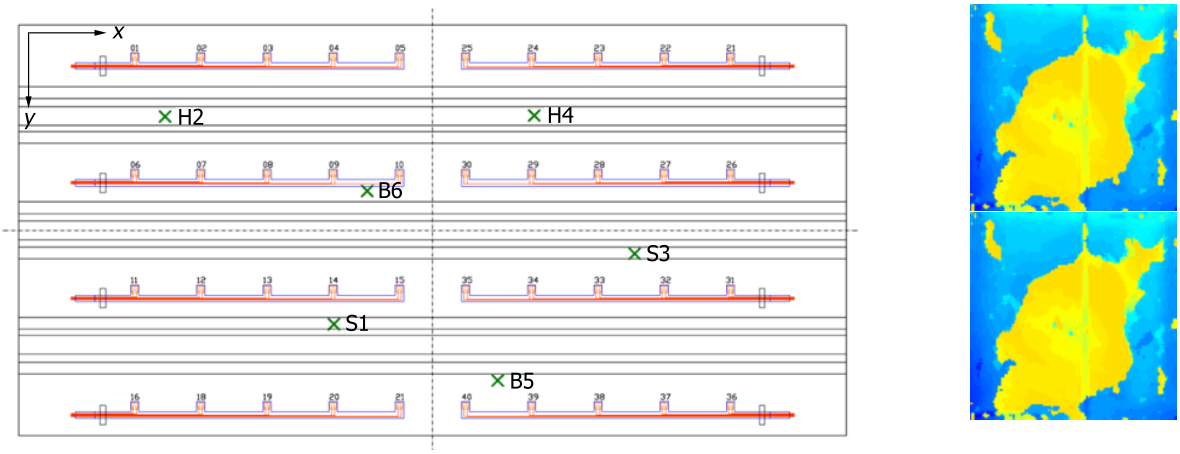

Figure 4: *Top view of the structure, indicating the location of stringers, transducers and impact locations (left) and two representative ultrasound scans of defects (right, top: H2; bottom H4) [9].*

Three different types of damage can be recognised. The distinction is made based on the relative position of the damage with respect to the Ω-stringers:

H-type Located under a stringer head

S-type Located under a stringer foot and target a debonding between stringer and skin

B-type Located on the skin between Ω-stringers and between transducers

The behaviour of the various damage types regarding the guided wave propagation is different in every case and are therefore subject of investigation.

3 SIGNAL PROCESSING

Raw measurement data, from a reference (pristine) state and a current state, is loaded in the damage assessment tool. The first step in the analysis is to apply a few signal processing steps. This paper does not intend to discuss the origin of some of the distorting effects that are filtered during the signal processing phase, but merely presents the solution as it is implemented. There are three important signal processing steps:

1. Distortion of first few measurement points
2. Zero offset
3. Electro-magnetic cross-talk

The first two are dealt with rather straightforwardly: The first few points (from experience, the default value is set to 5) are ignored by setting them to zero. Note that this corresponds to a time of 0.4 ns, given a typical sampling frequency of 12 MHz. The zero offset is corrected by subtracting the mean value of the entire signal (excluding the first few points that were already set to zero) from the signal. The electro-magnetic cross-talk poses more challenges. Without going in further details, it can be stated that the length of the part of the sensor signal that is affected by the cross-talk is related to the actuation frequency and the number of cycles in a burst - be it not directly. A pragmatic approach would be to simply ignore the part of the signal that is affected by the cross-talk. The following relation between the distance Δx_{PWAS} between two transducers and the actuation frequency f_{act} should be obeyed to allow this pragmatic approach:

$$\Delta x_{\text{PWAS}} > (n+m)\,\lambda = (n+m)\,\frac{v}{f_{\text{act}}} \tag{1}$$

with n being the number of cycles in the burst, m and arbitrary number to account for the uncertainty in starting point and the difference in number of cycles in the cross-talk signal, λ the wave length, and v the wave propagation velocity. Though this relation seems rather straightforward, the values of the various parameters exhibit a relatively large amount of scatter restricting the use of the higher actuation frequency. Hence, it is assumed to be inevitable that in some cases the real response of the sensor starts before the effect of the cross-talk has vanished.

There are various ways of implementing a filter. Principally, one can apply the filter in the frequency domain, in the time domain or in the time-frequency domain (e.g. using wavelets). The first corresponds for example with band filtering of the signal, the time domain filtering requires a reconstruction of the signal and generally an optimisation loop. Here a band pass filtering routine is implemented. It is assumed that the cross-talk signal mainly contains the actuation frequency. This is a reasonable, but not entirely correct assumption, as was shown by Moix-Bonet [11] in a technical report issued in the SARISTU project. The problem with using for example a time domain representation of the actuation signal is that the number of cycles in the cross-talk signal does not correspond to the number of cycles in the actuation signal (6 against 5 cycles). Filtering only the actuation frequency will leave some high frequency components behind, but these are small compared to the actual sensor signal. Evidently, the actuation frequency will also be present in the actual sensor response, leading to a part of the actual sensor signal being unintendently filtered in case there is overlap between the cross-talk signal and the actual sensor signal. The overlap, if present, is small, compared to the total length of the response signal, for the cases investigated, justifying the assumption that the filtering will not affect the damage identification. The filtering can be based on the part of the signal, after which the full signal is reconstructed assuming a certain level of symmetry of the cross-talk signal. A flow chart of the filter routine is presented in fig. 5.

First, the raw signal $s(t)$ is loaded and if cross-talk is detected, it is converted to the frequency domain $s(t) \rightarrow S(\omega)$. Subsequently, a low-pass filter is applied with a cut-off frequency f_c of (by default) 150% of the actuation frequency f_a. By default, the maximum ripple in the pass band ($f < fc$) is set to 1 dB, while an attenuation of 80 dB is used for the stop band ($f > fc$). The software allows to use different models for the low-pass filter - essentially, those offered by Matlab - and set all its parameters. The signal is transfered back to the time domain with an inverse fast fourier transformation after applying the low-pass filter ($S_{lpf}(\omega) \rightarrow s_{lpf}(t)$). Finally, the filtered signal is subtracted from the original signal, overwriting the original signal ($s(t) = s(t) - s_{lpf}(t)$).

4 DAMAGE ASSESSMENT

Once the raw data is processed, the damage identification algorithms can be applied. The approach followed corresponds with the signal correlation analysis technique as described by Su and Ye [3] and

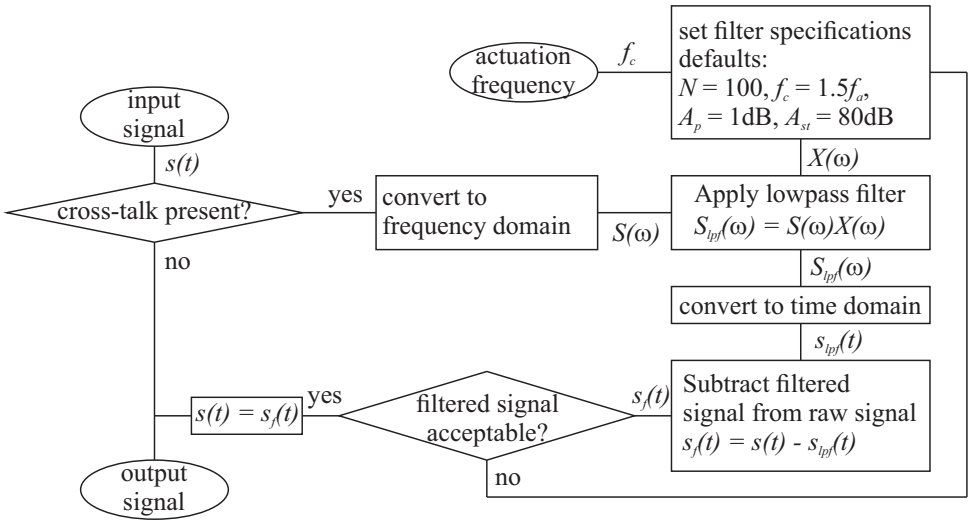

Figure 5: *Flow chart of the electro-mechanical cross-talk filter.*

the RAPID method [2]. However, a few adaptations are made by Moix-Bonet et al. [12] to improve the performance of the RAPID method.
First, a grid is defined, overlaying the panel. The damage intensity $I(x,y)$ at each grid point (x,y) is calculated, by assuming a certain area of influence of the actuator-sensor paths. The damage intensity if defined as [3]:

$$I(x,y) = \sum_{k=1}^{N_p} \left[(1-\rho_k) \left(\frac{\beta - R(x,y)}{\beta - 1} \right) \right] \tag{2}$$

with ρ_k being the correlation coefficient of the k^{th} actuator-sensor path, N_p the number of paths and β a scaling factor determining the area of influence. $R(x,y)$ is modified by Moix-Bonet et al. [12] by introducing the scaling factor α to modify the location of the probability distribution function and reads:

$$R(x,y) = \begin{cases} \dfrac{\sum\limits_{k=i,j} \sqrt{(\Delta x_k + q\alpha\Delta x_{nm})^2 + (\Delta y_k + q\alpha\Delta y_{nm})^2}}{(1-2\alpha)\sqrt{\Delta x_{nm}^2 + \Delta y_{nm}^2}} & \text{for } R(x,y) < \beta,\ q = \begin{cases} 1 & \text{for } k = i \\ -1 & \text{for } k = j \end{cases} \\ \beta & \text{for } R(x,y) \geq \beta \end{cases} \tag{3}$$

$$\Delta x_k = x - x_k, \quad \Delta y_k = y - y_k \quad \text{with } k = n, m; \quad \Delta x_{nm} = x_n - x_m$$

where (x_n, y_n) and (x_m, y_m) indicate the locations of transducer n and m respectively. Typically, β is equal to 1.05, but here, α and β are optimised based on minimisation of blind zones, of deviation in probability distribution values and of the kurtosis. The details of the optimisation are described in [12]. The values for α and β were found to be equal to 0.08 and 1.07 respectively. The resulting change distribution function is depicted in fig. 6.
Su and Ye [3] use the correlation coefficient ρ as an indicator of damage. The correlation coefficient equals unity if there is no damage and is lower than one if there is damage (since the correlation between the signals will be less). The correlation function is not the only possible indicator of damage: There are many methods to calculate a damage index (DI). Eleven methods [13] are implemented and tested on their performance next to the method based on the correlation coefficient. The damage indices are based on signal's intensity, time of an event (e.g. time of flight), frequency domain expressions, signal energy etc. In every method, attributes of baseline (healthy) and currently acquired (unknown health state) signals are compared, to identify potential change in the structural characteristics, which in turn would be an indication of damage. The performance depends on the type of damage (i.e. how the

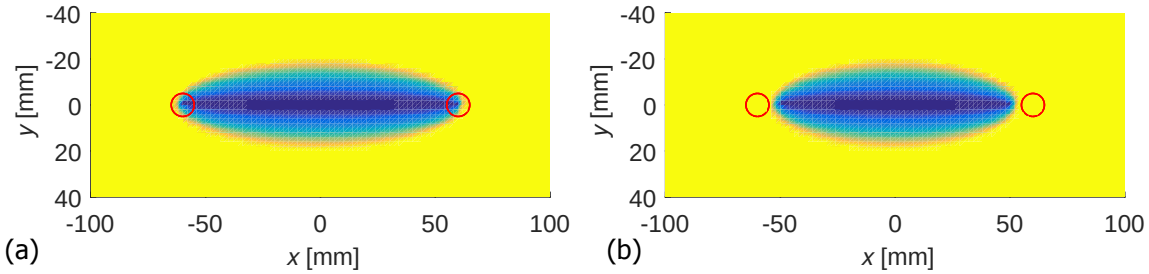

Figure 6: *Elliptical distribution function of influence for a):* $\alpha = 0$ *and* $\beta = 1.05$*; and b)* $\alpha = 0.08$ *and* $\beta = 1.07$ *as obtained after optimisation [12].*

signal is affected) and on the actuation frequency. It is therefore difficult, if not impossible, to formulate definite conclusions on the performance.
The methodologies implemented, along with their mathematical formulas, are presented in table 1. The damage assessment software allows the user to mutually compare methods and select the best performing method for the case under investigation or to use a combination of methods. An issue to address is that the damage index that is calculated in most methods gives a value of zero if no damage is present and some nonzero value, generally above unity, if there is damage. The following relation applies between the value of the correlation coefficient and the damage index:

$$\rho_k = \frac{1}{DI + 1}, \quad DI = \rho_k^{-1} - 1 \tag{4}$$

The only exceptions are the Signal Amplitude Peak Ratio (SAPR) method and the Ratio of Covariance Matrix Eigenvalues (RCME) method. In case of the SAPR method, the damage index equals 1, rather than 0 in case of no damage, but also tends to infinity in case of damage: the '+1' in the denominator of the first equation in (4) is dropped. The RCME method in gives a value between 1 and 0 for the healthy and damaged state respectively, like the correlation coefficient. Using (4) allows to use any damage indicator in combination with the damage intensity $I(x, y)$ as defined in (2).

5 SOFTWARE WITH GRAPHICAL USER INTERFACE

The routines to convert the raw data signals to a coloured plot of the damage intensity $I(x, y)$, indicating possible damage locations, are embedded in a software package with a graphical user interface (GUI). The user can quickly analyse a set of measured responses without having to be an expert in the signal processing and damage identification algorithms. It is however also possible to tune many of the variables, allowing a more experienced user to perform a more detailed analysis of the data.
Both experimental and numerical data can be analysed with the GUI. It is therefore for example possible to run a series of numerical analysis to investigate the effect of specific damage characteristics on the capability of the damage identification process. A better understanding of these effect will enhance the interpretation of experimental results. However, in this paper only experimental results are shown.
The GUI is structured in three sections: a section with buttons to toggle between the different user control panels; a section for the user control panels; and a section for graphical representations. There are five different user control panels, overlaying each other and allowing the user to control the operations applied to the data: the file load panel, the preprocessor panel, the algorithms panel, the data visualisation panel and the export panel.
The software is developed to handle different types of input. Data that can be loaded is experimental data from the ScanGenie system (Acellent Technologies Inc.) as used by the DLR and especially Airbus, experimental data from measurements from the University of Siegen and numerical data from the models from the University of Siegen and the University of Patras. The format of the data is different. Hence, the user first needs to select the type of data.
The signals from the transducers are restructured to obtain a memory efficient and logical structure. The memory efficiency is significantly higher than the default structure of the ScanGenie Matlab export;

Table 1: *Damage identification algorithms implemented in the damage assessment software.*

	Method Name	Abbr.	Mathematical Formula
1	Correlation Coefficient	CC	$\rho = \frac{\sum_{i=1}^{N}(S_{H,i}S_{D,i}) - \sum_{i=1}^{N}(S_{H,i})\sum_{i=1}^{N}(S_{D,i})}{\sqrt{\sum_{i=1}^{N}(S_{H,i}^2) - \left(\sum_{i=1}^{N}(S_{H,i})\right)^2}\sqrt{\sum_{i=1}^{N}(S_{D,i}^2) - \left(\sum_{i=1}^{N}(S_{D,i})\right)^2}}$
2	Signal Amplitude Peak Ratio	SAPR	$DI = \frac{\max(S_H)}{\max(S_D)}$
3	Signal Amplitude Peak Squared Percentage Differences	SAPS	$DI = \left(\frac{\max(S_H) - \max(S_D)}{\max(S_H)}\right)^2$
4	Signal Amplitude Hilbert Transform Maximum	SAHTM	$DI = \left\lvert\frac{\max(\boldsymbol{H}(S_H)) - \max(\boldsymbol{H}(S_D))}{\max(\boldsymbol{H}(S_H))}\right\rvert$
5	Signal Sum of Squared Differences	SSSD	$DI = \frac{\sum_{i=1}^{N}\left[(S_{H,i} - S_{D,i})^2\right]}{\sum_{i=1}^{N}\left[S_{H,i}^2\right]}$
6	Welch-based Power Spectral Density	WPSD	$DI = \frac{\left\lvert\int_{f=0}^{2f_{\text{act}}} \boldsymbol{PW}(S_D)\mathrm{d}f - \int_{f=0}^{2f_{\text{act}}} \boldsymbol{PW}(S_H)\mathrm{d}f\right\rvert}{\int_{f=0}^{2f_{\text{act}}} \boldsymbol{PW}(S_H)\mathrm{d}f}$
7	Welch-based Transfer Function	WTF	$DI = \frac{\left\lvert\int_{f=0}^{2f_{\text{act}}} \boldsymbol{TF}(S_D)\mathrm{d}f - \int_{f=0}^{2f_{\text{act}}} \boldsymbol{TF}(S_H)\mathrm{d}f\right\rvert}{\int_{f=0}^{2f_{\text{act}}} \boldsymbol{TF}(S_H)\mathrm{d}f}$
8	Cross Correlation Time-of-Flight Percentage Difference	CCToFPD	$DI = \frac{\lvert\operatorname{argmax}(\gamma_H) - \operatorname{argmax}(\gamma_D)\rvert}{\operatorname{argmax}(\gamma_H)}$
9	Cross Correlation Maximum Percentage Difference	CCMPD	$DI = \frac{\lvert\max(\gamma_H) - \max(\gamma_D)\rvert}{\max(\gamma_H)}$
10	Hilbert Transform based Time-of-Flight Percentage Difference	HToFPD	$DI = \frac{\lvert\operatorname{argmax}(\boldsymbol{H}(S_H)) - \operatorname{argmax}(\boldsymbol{H}(S_D))\rvert}{\operatorname{argmax}(\boldsymbol{H}(S_H))}$
11	Discrete Wavelet Transform Approximation Coefficients	DWTAC	$DI = \frac{\sum_{i=1}^{N}\left[(\boldsymbol{DWT}(S_{H,i}) - \boldsymbol{DWT}(S_{D,i}))^2\right]}{\sum_{i=1}^{N}\left[(\boldsymbol{DWT}(S_{H,i}))^2\right]}$
12	Ratio of Covariance Matrix Eigenvalues	RCME	$\rho = 1 - \frac{\lambda_2}{\lambda_1}$

this contains a fair amount of redundancy, since the actuator signal is stored for each path, also if the sensor signal from another path is obtained from the very same actuator signal. In general, a number of transducer act as sensor each time a transducer is acting as actuator. All sensor signals of a single actuation cycle are saved together with the actuator signal of that cycle. This avoids redundancy and in the end allows the user to load multiple cases at once, without running in to memory related errors or slow functioning of the computer. This is of particular interest when analysing full-scale structure such as the door-surrounding structure.

The signal processing steps described in section 3 of this paper can be activated in this part of the software. The user can decide to skip these, as for example the numerical data does not show electro-magnetic cross-talk. It is also possible to change settings of the signal processing steps, although it is recommended to follow the default settings if one is not familiar with the signal processing concepts.

The cross-talk filter takes the largest part of the preprocessor panel. Most graphical elements are related to settings of the filter, and will not further be addressed here. It is however important to note that the

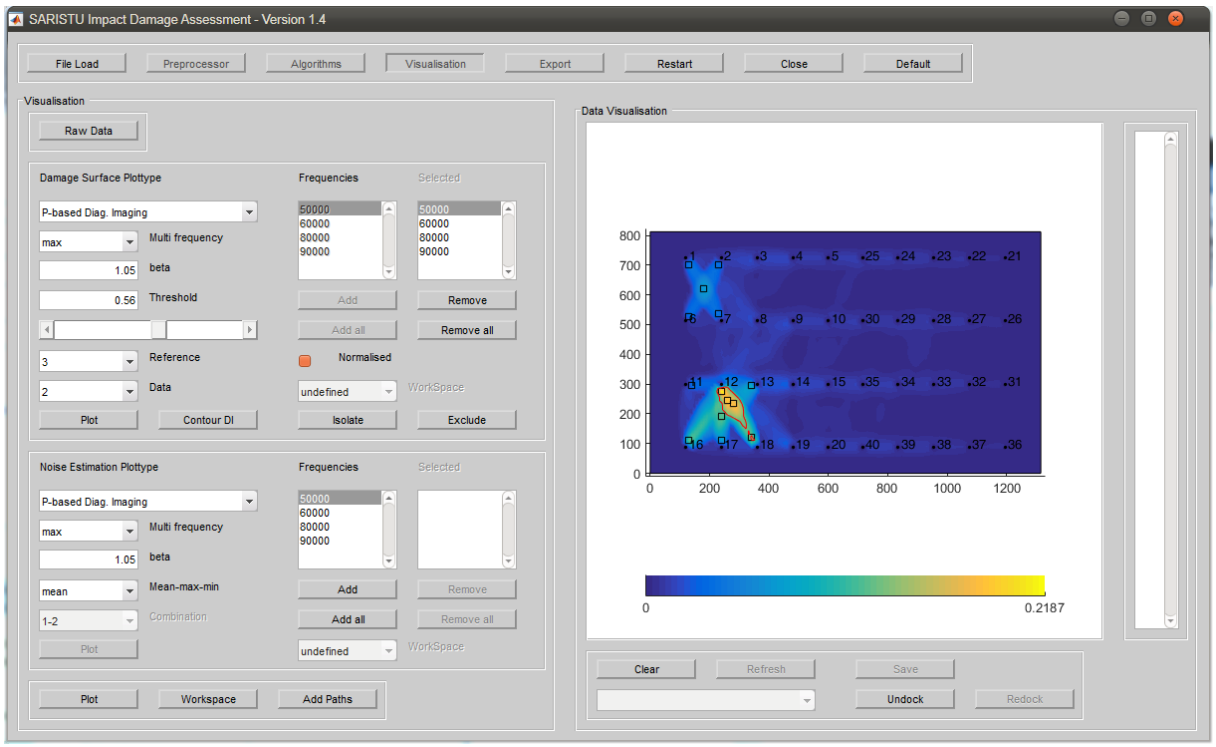

Figure 7: *The graphical user interface with on the top the menu toggle buttons, the user control panel on the left (active control panel:data visualisation) and the graphical display area on the right. The plot shows the damage intensity $I(x,y)$ for the curved plate with a DuraAct™ PWAS sensors. The red line indicates the threshold, set here at 0.56. The square markers indicate peaks in the damage intensity.*

filtering is first applied to a copy of the data and shown to the user in the graphical visualisation panel on the righthand side of the GUI. The filter is only applied upon acceptance by the user; the original data is overwritten by the filtered data and the temporary data is deleted.

Finally, the grid for the damage plot has to be created. The default is a (nearly) square grid, with a density based on the dimensions of the workspace; the number of elements must be an integer number and therefore the edge lengths are set as close as possible to a square grid by default. The ratio of the grid dimensions can also be unconstrained - resulting in a rectangular grid - and the grid can be based on edge size rather than on a number of elements in each direction. Again, the edge lengths are adjusted to obtain the nearest integer number for the number of elements along the domain edge.

Once the data has passed through the necessary signal processing steps, a damage identification method can be selected. A popup menu in this panel provides the possibility to select one of the algorithms listed in table 1. The damage identification algorithms are applied to all combinations of reference and current data sets. If multiple reference data sets are used, the difference between these data sets can also be analysed, which gives an estimation of the noise of the measurements. The ratio of the damage probability, expressed by the values of the damage intensity, $I(x,y)$, over the noise level is a criterion for the performance of the methods, as will be discussed in section 6.2. The same algorithms are used for this noise estimation as are used for the damage identification and again all possible combinations of data sets are analysed.

Various aspects can be shown in the graphical representation area. First of all, the geometry can be shown. This means the geometry of the entire panel, but also that of (one of) the workspace(s). If a workspace is selected, the paths can be added to the plot.

Secondly, the raw data can be plot. The term 'raw' here refers to the time data of the transducers that is stored, after the signal processing (if applied). The actuator and sensor signals are separated as are the reference and current state data, resulting in a set of four graphs. The raw data plot is the only plot

that can be made if no reference data is loaded. In that case only two graphs are shown.
The largest sub-panel is the damage surface plot section. The damage intensity $I(x, y)$ is plot as a coloured surface plot, using (2) and (3) (fig. 7). The colour indicates the intensity, where blue refers to a low intensity (no damage) and yellow to a high probability of damage. The absolute values of the damage intensities are given in the colourbar. It is possible to show the intensity for specific actuation frequencies, if multiple actuation frequencies are used. Note that in general only a single actuation frequency is used per actuator, such that an incomplete path coverage is obtained if not all actuation frequencies are included. The user can choose to plot the maximum, mean or minimum intensity in case multiple damage indices (multiple actuation frequencies) per path are available.
The intensity gives an indication of possible damage locations. However, it is up to the user to set a threshold, as the absolute value of the damage intensity depends on many variables, such as the type and location of the damage or the presence of other damages. No physical interpretation is available to set a general threshold. A slider can be used to set the threshold. If a threshold is set, dynamic contour lines are plot, indicating the border between the intensities below and above the threshold. The contour lines are updated each time the threshold is changed. A potentially damaged area can be selected by choosing a proper threshold value. Square markers are added as well, indicating peaks in the damage intensity. A peak is defined as a damage intensity value that is higher than the damage intensity of all its surrounding points and higher than a preset (hard-coded) threshold. Once the threshold is set, an area enclosed by a contour can be selected (note that multiple contours can be present). The damage index of the area is subsequently stored. The user can now either focus further on the area enclosed in the contour, by isolating it, or focus on other areas by excluding this. The colour scaling of the intensity is updated after isolation or exclusion of the area enclosed by the contour. Thus, in case of the latter, secondary potentially damaged areas can more easily be identified: this procedure offers unique possibilities for assessing multiple damages in the structure.
The damage intensity indicates possible locations for the damage: to investigate the likelihood that it concerns a real damage, the data needs to be exported and subsequently imported in a Probability of Detection (PoD) analysis. Prior to be allowed to enter the data export panel, at least one damaged area must be identified, by setting a threshold for the damage intensity and selecting an area enclosed by a contour. Two different export files, both in ASCII format can be exported:

1. Data file containing information on the damage intensity in the contour(s) selected
2. Data file containing the damage indices for each path

The files start with a header providing information on the data files used and the date the file was created and the dates it was appended (if). The damage extent file then contains by default four elements for each contour that is exported:

1. The damage intensity integrated over the area enclosed by the contour
2. The area enclosed by the contour
3. The coordinates of the peaks in the contour and their values
4. The centre coordinates of all grid elements in the contour and their damage intensity value

An integrated value of the damage intensity is preferred, since the damage will in reality also cover an area. Taking the highest peak and assuming a specific radius based on for example the peak height does not necessarily reflect the information present in the damage intensity. On the other hand, the location of the peaks in the contour area is related to the location of the crossings of the paths, rather than to the real damage.
The damage path file contains per path in a workspace the following information:

- The transducer number of the actuator and that of the sensor
- The actuation frequency
- The damage index of the path

- The x- and y-coordinates of the actuator and those of the sensor
- The length of the path

For both types of exports, the user can control which of the items are included in the export file.

6 DISCUSSION

The objective is to assess a damage identification method. The GUI is an integral part and therefore not only the performance of the damage identification algorithms is assessed, but also the functionality of the GUI, in particular how it helps in the analysis of a potentially damaged panel.
The damage identification GUI is used to analyse a number of damage cases, as indicated in section 2. The response to the damage depends on a combination of actuation frequency and its location (H-, S-, B-type). A concise discussion based on the more elaborate analysis from Moix-Bonet et al. [12] is therefore included. At the end of the section, the results obtained on a full-scale door-surrounding structure will be shown.

6.1 Actuation Frequency

The damage assessment is performed on the one hand with signals acquired in a frequency range between 60 kHz and 90 kHz, where the asymmetric fundamental mode (A_0) is dominant according to the theory of mode tuning presented by Giurgiutiu [14]. On the other hand, an assessment is performed with signals acquired in a frequency range between 200 kHz and 250 kHz. In this frequency range, the symmetrical fundamental mode (S_0) has a dominant role.
The accuracy of both frequency ranges is illustrated by analysing damage H4 (see fig. 4). The estimated location of the damage is compared to the damage location as obtained via traditional nondestructive inspection (in this case ultrasound inspection). The SAPS and CC damage identification algorithm (see table 1) are used for the low and high frequency ranges respectively, as they were revealed to provide the best results. The estimated locations (x, y) are presented in table 2. The estimated area A is also given, as is the threshold I_{thrs} set for the contour line. Note that the threshold is set as a percentage of the range of damage intensities for each case.

Table 2: *Comparison of the estimated damage location (x, y) and area A based on conventional NDI and the low (A_0-dominant) and high (S_0-dominant) frequency cases [12].*

	I_{thrs} [%]	x [mm]	y [mm]	A [mm^2]
NDI		835	618	574.06
A_0 mode	95	833.2	621.5	586.9
S_0 mode	94	833.2	531.3	25.1

Clearly, the presence, location and area of the damage is more accurately identified if the A_0 mode is used. The criteria to select the most appropriate frequencies were the amplitudes of the received signal at those frequencies and the isolated first arrival of the wave packet. The amplitude between 200 kHz and 250 kHz appeared to be sufficiently high (though increases rapidly between 250 kHz and 300 kHz), as is shown in fig. 8. However, the mode density is high, compromising the second criterion and also hindering the damage detection with the damage identification algorithm selected.
It can also be argued that the A_0 fundamental mode is more sensitive to a delamination type of damage than the S_0 fundamental mode. The A_0 mode will open and close the delamination, whereas the delamination stays more closed if an S_0 mode is passing. On the other hand, the amplitudes of the asymmetric fundamental mode tend to be lower compared to the symmetric fundamental mode, reducing their sensitivity. It is difficult to state firm conclusions on the best frequency to use, due to the complexity of the geometry. The GUI allows a fast assessment of the performance of the various identification methods for various actuation frequencies - if, evidently, they were included in the measurements.

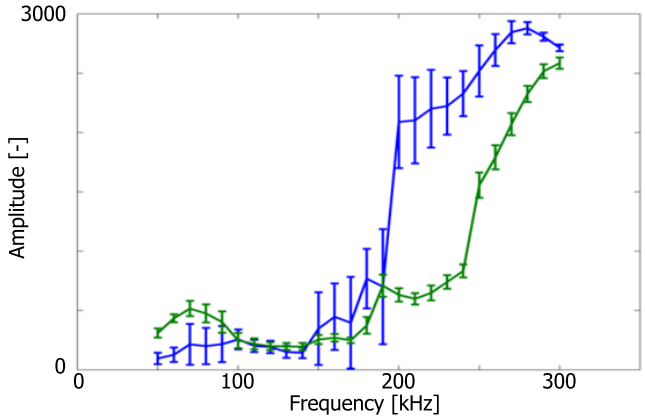

Figure 8: *Acquired maximum amplitudes, mean and deviations, with the SMARTLayer® (blue) and DuraAct™ (green) for a single path parallel to a stringer (length 120 mm) [12].*

6.2 Damage Index Selection

In [12], the suitability of the damage identification algorithms is analysed based on the ratio of probabilities of the damaged over the undamaged case and the error in the damage localisation. The first criterion is a measure for the sensitivity of the damage index in relation to the noise level. The ratio compares the maximum damage probability obtained with the identification algorithm for two baselines (no damage) with the maximum probability acquired for a damaged case. The damage localisation error is defined as the difference of the x- and y-coordinates of the center of the damage obtained with traditional NDI (here ultrasound) and the coordinates obtained using the identification algorithm. It was found [12] that four damage identification show a low sensitivity for all damage types and two more can be discarded based on the high error in localisation. These methods depend on the cross-correlation, the Hilbert transform and the Welch transfer function. The Hilbert transform is equally sensitive to defects as it is to noise and is therefore not applicable for damage identification. The Welch transfer function is based on the spectral density. However, it is very challenging to find changes in a complex signal with multiple wave packets, solely considering the frequency domain information, since the multiple wave packets present in the signal are effected differently by the presence of damages. Finally, the cross-correlation performed on the entire signal cannot be representative for damage identification purposes, since time or phase shifts are not uniform throughout the signal.
The remaining damage identification algorithms that effectively identify and locate damage are based on the maximum amplitude (SAPR and SAPS) or amplitude over the whole signal (SSSD and DWTAC). The covariance matrix (RCME) and the correlation coefficient (CC) also proved to be sensitive. The algorithm that performs best may differ from case to case, even within a single panel (e.g. different damage type). Therefore, the damage intensity can be based on a combination of damage identification algorithms. Once again, the GUI offers a easily accessible method to analyse the effectiveness of different algorithms - either separate or combined - without requiring the user to have detailed knowledge on these algorithms.

6.3 Full scale door-surrounding structure

The final test of the software is whether it can deal with large amounts of data as will be found in full scale applications such as the door surrounding structure that was manufactured in the framework of the EU FP7 project SARISTU [10]. 584 transducers were integrated in the structure leading to a data set of 1698 path signals measured for one half of the structure per actuation frequency. Only one half could be measurement each time, due to limitations in the number of channels of the data acquisition channel. The total amount of data loaded into the software is equal to twice that of a single measurement, since

the algorithms are based on a comparison to a reference state. In an initial test, a mass (tacky tape, $m \ll m_{\text{total}}$) was stuck to the structure. A single actuation frequency of 60 kHz was used. The resulting damage intensity is shown in fig. 9.

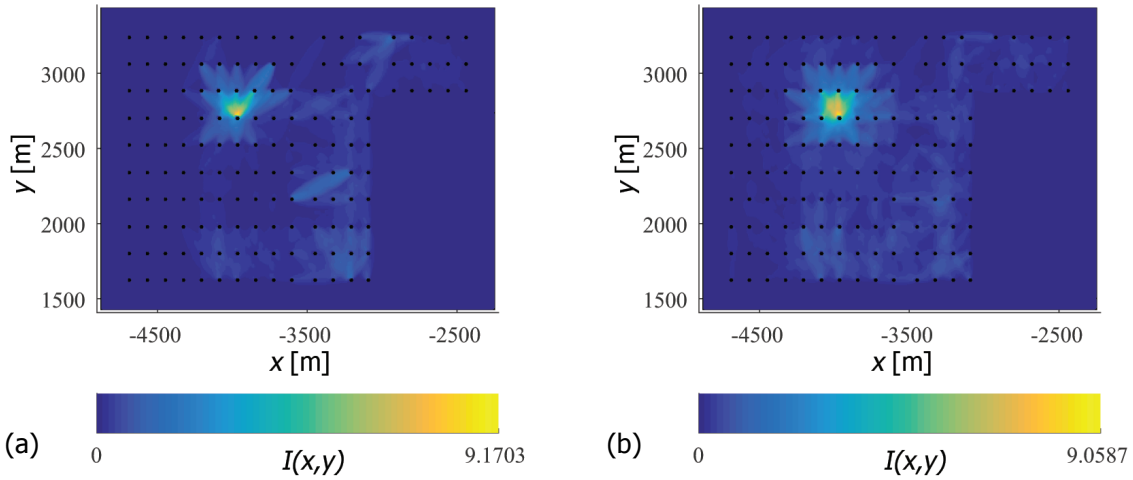

Figure 9: *Damage intensity of the door surrounding structure with a small mass as damage case. Two damage identification algorithms: a) Correlation Coefficient and b) Signal Amplitude Peak Ratio.*

The first observation is that the location of the mass is predicted correctly. A quantitative analysis is not performed on this case, as the main objective was the analysis of the functionality of the software with data sets of this size. The software turned out to function without problems, despite some slow processing of the graphics (a known issue with Matlab) and a relatively long time ($\sim$400 s) needed for applying the cross-talk filter. No particular slowness of the software due to memory constraints was noticed. A standard laptop was used (HP Elitebook 8530W, Intel(R) Core(TM)2 Duo CPU T9600, 2$\times$2.80 GHz, 4 GB RAM, 64-bit operating system). This example shows the software is able to deal with data sets from realistic structures.

7 CONCLUSIONS & FUTURE PROSPECTS

The damage identification method that is developed has proven to be effective: algorithms and actuation frequencies were analysed and selected, based on their performance to identify (localise) various types of damages. The GUI is an essential part in this analysis, in facilitating sense. However, it also paves the road for on-site damage analysis: the user of the software does not need to be an expert in the data analysis elements included in the software. The results obtained here, are mostly generated using the software in its present form. However, the development of the software has ran parallel to the development of the algorithms - a process that is still continuing.
Currently, the door surrounding structure is subjected to tests, comprising baseline measurements and measurements after a large series of impact loads have been applied to the structure. The analysis of the large amount of data will be greatly served by the damage identification GUI. At the same time, it will be an important test for the functionality of the software. Once the software has passed this test successfully, a stand-alone version of the software can be developed to allow for even more easy use (currently restricted to application in a Matlab environment).

ACKNOWLEDGEMENT

The research leading to these results has received funding from the European Union's Seventh Framework Programme for research, technological development and demonstration under grant agreement no 284562.

REFERENCES

[1] I. Buethe, N. Dominguez, H. Jung, C.-P. Fritzen, Ségur D, and F. Reverdy. Path-based mapod using numerical simulations. In *Proceedings of the SARISTU End of Project Meeting, Moscow*, page 8. Springer, 2015.

[2] H. Gao, Y. Shi, and J.L. Rose. Guided wave tomography on an aircraft wing with leave in place sensors. *Review of Quantitative Nondestructive Evaluation*, 24:1788–1795, 2005.

[3] Z. Su and L. Ye. *Identification of Damage Using Lamb Waves – From Fundamentals to Applications*, volume 48 of *Lecture Notes in Applied and Computational Mechanics*. Springer, 2009.

[4] H. Matt, I. Bartoli, and F. Lanza di Scalea. Ultrasonic guided wave monitoring of composite wing skin-to-spar bonded joints in aerospace structures. Technical report, NDE & Structural Health Monitoring Laboratory, Department of Structural Engineering, University of California, San Diego, 2005.

[5] X. Zhao, H. Gao, G. Zhang, B. Ayhan, F. Yan, C. Kwan, and J.L. Rose. Active health monitoring of an aircraft wing with embedded piezoelectric sensor/actuator network: I. defect detection, localization and growth monitoring. *Smart Materials and Structures*, 16:1208–1217, 2007.

[6] Z. Wu, K. Liu, Y. Wang, and Y. Zheng. Validation and evaluation of damage identification using probability-based diagnostic imaging on a stiffened composite panel. *Journal of Intelligent Material Systems and Structures*, page 1045389X14549873, 2014.

[7] D. Schmidt. CFRP panel with integrated SHM network. Technical Report SARISTU technical report, DLR, 2013.

[8] M. Moix-Bonet, I. Buethe, M. Bach, C.-P. Fritzen, and P. Wierach. Durability of co-bonded piezo-electric transducers. *2nd International Conference on System-Integrated Intelligence, Procedia Technology*, 15:639–648, 2014.

[9] M. Moix-Bonet, P. Wierach, R. Loendersloot, and M. Bach. Damage assessment in composite structures based on acousto ultrasonics - evaluation of performance. In *Proceedings of the SARISTU End of Project Meeting, Moscow*, page 10. Springer, 2015.

[10] D. Schmidt, A. Kolbe, R. Kaps, P. Wierach, S. Linke, S. Steeger, F. v. Dungern, J. Tauchner, C. Breu, and B. Newman. Development of a door surrounding structure with integrated structural health monitoring system. In *Proceedings of the SARISTU End of Project Meeting, Moscow*, page 8. Springer, 2015.

[11] M. Moix-Bonet. Guidelines for the signal processing algorithm. Technical Report SARISTU technical report, DLR/Airbus Innovations Group, 2012.

[12] M. Moix-Bonet, B. Eckstein, R. Loendersloot, and P. Wierach. Identification of barely visible impact damages on a stiffened composite panel wit a probability-based approach. In *Proceedings of the International Workshop on Structural Health Monitoring, Stanford, USA (accepted for oral presentation)*, 2015.

[13] P.G. Michaelides. Pitch catch algorithms preliminary analysis. Technical Report SARISTU technical report, 2013.

[14] V. Giurgiutiu. Tuned Lamb wave excitation and detection with piezoelectric wafer active sensors for structural health monitoring. *Journal of Intelligent materials systems and structures*, 0:291–305, 2005.